MULTISCALE SIMULATION OF UNIDIRECTIONAL CARBON FIBER REINFORMCED POLYMER STRENGTH

Hayden Cornwell, Luiz Lima, Flavio Souza

MultiMechanics
Omaha, NE, USA

ABSTRACT

Finite element (FE) analysis has become increasingly important for mechanical design and the development of new advanced materials. Being able to predict structural performance accurately and efficiently can circumvent the extensive time and cost of repetitive and rigorous material testing. However, with fiber reinforced polymers (FRPs), the assumption of homogeneity as well as the generalization of a material based on global properties does not sufficiently describe the material close to failure. The key to accurately predict component failure is to realistically capture microstructural damage under complex multiaxial loads while simultaneously relaying the material response to the part level. This is possible through TRUE multiscale analysis (similar to FE^2 but with a drastic reduction in computational cost) and in this paper, is applied to a specific FRP, unidirectional (UD) carbon fiber reinforced polymer (CFRP). The first study demonstrates the benefit of stochastic variance at the microstructure length scale. Multiple representative volume elements (RVEs) are created with varying fiber volume fraction (FVF), slight fiber misalignment, and the fiber strength following the Weibull statistical distribution. These different RVEs are applied to a coupon, tested in longitudinal tension. Multiple runs of this multiscale model result in varying strengths and moduli due to the stochastic nature of the model. These results are compared against the experimental results this model is based on, showing good agreement. The second study uses a different RVE (representing the same UD CFRP), integrated in a model of a laminate with multiple plies in different orientations. The RVE's constituent material properties (fiber, matrix, and fiber-matrix interface properties) are designated using only standard lamina level data. After the RVE is calibrated, three different laminate models for each material are run with the results showing stress-strain curve and strength of the coupon. These results are well aligned within experimental data publicly available through the National Institute for Aviation Research (NIAR), demonstrating the accuracy of failure prediction using multiscale simulation. All models were run using the multiscale simulation software MultiMech.

1. INTRODUCTION

The adoption of Fiber Reinforced Polymers (FRP) in industries such as aerospace and automotive shows an increasing trend in the previous decades. The benefits of applying these materials as a replacement for traditionally-used metallic alloys include weight reduction, durability, and design flexibility. These composites also become more and more appealing as manufacturing costs and raw material prices decrease [1].

Copyright 2019. Used by the Society of the Advancement of Material and Process Engineering with permission.

SAMPE Conference Proceedings. Charlotte, NC, May 20-23, 2019. Society for the Advancement of Material and Process Engineering – North America.

The mechanical behavior of FRP materials is not straightforward, mainly due to the complexity of the microstructures and the highly non-linear behavior of the polymers used as the matrix. Analytical methods and numerical tools based on such methods were developed to support and facilitate FRP design. These methods are generally sufficiently accurate to make predictions about the stiffness and the general elastic behavior of the FRPs [2-3]. However, analytical formulations to predict the failure of composites are generally inaccurate. This is because these failure criteria use simple experimental lamina level data (like longitudinal, transverse, and shear strength) to create a failure envelope for the transversely isotropic material. [4-7].

New material models adopting different and more complex methodologies, like progressive failure, that have shown promise in predicting composite failure under certain loadings, do not demonstrate the same fidelity in other load cases [8-13]. Another struggle in predicting absolute strength in FRPs lies in the stochastic nature of this family of material. Along with varying fiber volume fraction (FVF), fibers inherently follow a Weibull strength distribution. Fiber breaks result in stress concentrations that promote more fiber resin debonding and resin cracking, causing further microstructural damage [14-16].

A recent alternative to address the flaws in the traditional analytical methods is the development of multiscale numerical tools, in which both the part and the microstructural scales are solved by finite-element (FE) simulations, in a coupled fashion. Hence, the strain levels in the part are sent as inputs to a FE solution in the microstructure scale, at each time increment [17-19]. Failure mechanisms originating in the micro-scale due to these strains are captured and the effects are upscaled back to the part level. This procedure allows for a more accurate prediction of the material strength, as only minor simplifications are assumed, in comparison to the ordinary analytical solutions.

This paper describes two studies focused on the application of multi-scale numerical solutions in tensile tests of unidirectional (UD) carbon fiber reinforced polymers (CFRP). The simulations were executed using the software MultiMech 18.1, which accounts for the realistic response of the microstructure in the full-scale coupon by including the representative volume element (RVE) as the material for the global scale model, allowing the simulation of both finite element models at the same time, in an embedded manner. The first study investigates the influence of non-uniformities in the specimen by the strength of CFRP coupons under tension, by considering differences in FVF, alignment, and fiber strength of the representative volume elements (RVEs) used to model the microstructure. In the second study, the same CFRP RVE is calibrated based on standard lamina level data, and this microstructure is applied to standard National Institute for Aviation Research (NIAR) tensile test coupons. The strength calculated by numerical methods is then compared to the results stated in the standard.

2. NUMERICAL MODELING

2.1 Study #1

The coupon considered in this study is described by Malgioglio [20]. It consists of a standard tensile test coupon, with dimensions 10.5 x 3.5 x 0.28 mm, discretized in 30,000 finite elements. Two types of heterogeneities are considered in the coupon scale: alignment and volume fraction. Misalignments were measured experimentally, as described by Sutcliffe [21], and applied to the

finite-element model, so that each element has a different level of misalignment, both in the in-plane and out-of-plane directions. In a multiscale model, the misalignment is included by rotating the coordinate system of the element in the coupon scale, whose strains are used as input for the RVE scale model. Seven different volume fractions were considered, ranging from 0.3 to 0.6, with a different RVE being used for each bundle. This is depicted in Figure 1.

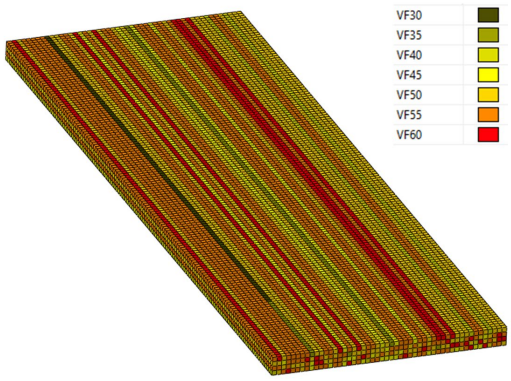


Figure 1. Distribution of fiber volume fraction in the microstructure throughout the FE test specimen.

The composite considered in this study is Hexcel IM7/8552 carbon epoxy prepreg, which was evaluated in detail by NIAR [22]. An example of the RVEs created is shown in Figure 2 (in this case, a 60% fiber RVE), with relative dimensions of 25 x 25 x 10. There are no differences in microstructure properties when comparing RVEs with and without fibers intersecting the transverse boundaries. The 8552 resin was considered as a linear elastic material, with a Young's modulus of 4670 MPa and a Poisson's ratio of 0.4.

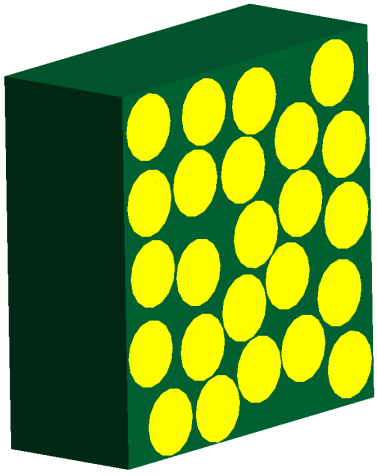


Figure 2. Visualization of the 60% fiber RVE, showing the resin (green) and the fibers (yellow).

The carbon fiber was defined as an orthotropic elastic model with its main mechanical properties given in Table 1. Additionally, a stochastic failure parameter was considered, ruled by a Weibull distribution which causes each element of the fiber to fail at a different load. This simulates the natural inhomogeneity of the material. Figure 3 shows the distribution of probability of failure as a function of the maximum principal stress. Internally, this distribution is ruled by Equation 1:

$$P_{failure}(\sigma_e) = 1 - \exp\left[-\frac{V_e}{V_s}\left(\frac{\sigma_e}{\sigma^f}\right)^m\right] \quad [1]$$

where V_s is the scale parameter, m is the shape parameter, σ^f is the nominal limit of maximum principal stress, σ_e is the maximum principal stress in the element and V_e is the reference volume of the element. The volume ratio is a criterion included to account for the known relation between specimen size and failure probability.

Table 1. Elastic properties of the orthotropic model used for the fiber.

Young's modulus – fiber direction (GPa)	298
Young's modulus – transverse direction (GPa)	19
Shear modulus 12/13 (GPa)	27.6
Shear modulus 23 (GPa)	12.88
Poisson's ratio 12/13	0.2
Poisson's ratio 23	0.35

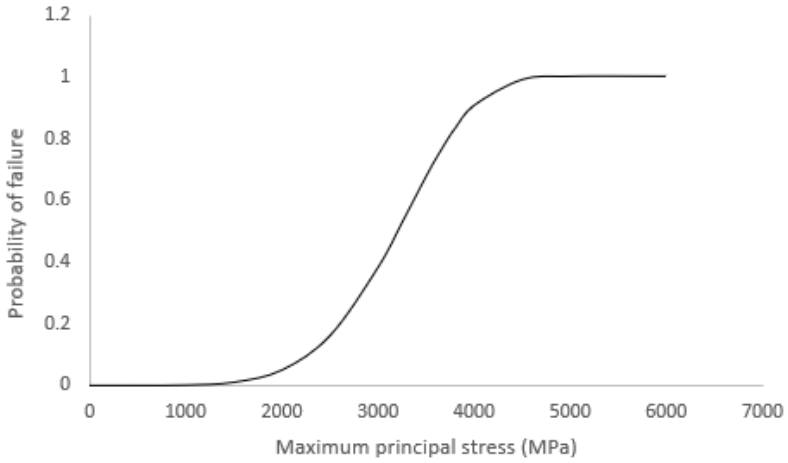


Figure 3. Probability of fiber failure as a function of element maximum principal stress.

The virtual coupon was submitted to three tensile tests, in order to verify the change in strength due to the stochastic variation of the fiber strength in each of the simulations. Each test utilized a different randomness seed, which redistributed the element strengths for the different tests. The specimen was loaded in tension to a strain level of 0.22, enough to promote failure in the three simulations executed in sequence.

2.2 Study #2

In the second study, three unnotched tensile tests described by NIAR [22] are reproduced using the same multiscale numerical methodology. Each element of the coupon-scale mesh considers an RVE with 60% FVF. As in the first study, the fiber is considered as IM7, while the resin is 8552. However, unlike the unidirectional case, the RVE will be rotated to the specified layup angles for the different tensile tests. To accurately characterize the multidirectional failure of the material, a different approach was taken to obtain the material properties for each of the microconstituents. First, a more simplified microstructure was used, as seen in Figure 4. Then, a 6-step calibration procedure was followed to gather the main mechanical properties of the materials, based only on standard lamina data for the composite, given in Table 2.

In addition to the lamina data, some assumptions were considered in the calibration process:

- The G23 shear modulus of the fiber is assumed to be 30% the value of the G12/G23 shear modulus;
- The Poisson's ratio of the resin is assumed to be equal to 0.35;
- The fiber is assumed to fail following a failure model based on the value of the maximum principal stresses. Due to the simplicity of the RVE, a Weibull strength distribution was not used. This was to ensure a sudden failure of the specimen, as seen in experimental data.
- The interphase is assumed to fail following a Weibull maximum stress failure model. This was to ensure the transverse failure of the composite demonstrated progressive failure.
- Before a constituent material property is calibrated, place holder values based on material heuristics are used. Because of the uniaxial tests utilized for this calibration, the material parameters of interest govern the composite properties, eliminating dependence on other constituent material parameters. For example: the fiber longitudinal modulus dominates the composites longitudinal modulus, so other material parameters can be assumed.

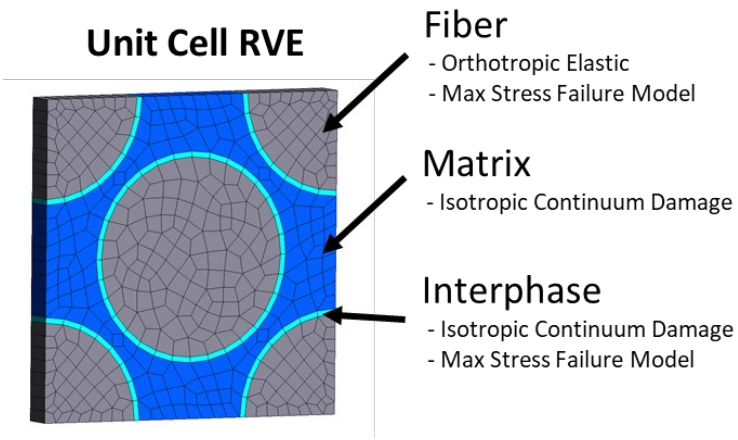


Figure 4. Description of the RVE used in study #2.

The steps listed below show the calibration step, the target lamina parameter, and the microconstituents material that is being calibrated, respectively. In every case, the RVE is loaded in a uniaxial manner to gauge the specified lamina parameter in Table 2 (in section 3.2). The microconstituent material parameter behaves as a variable and is changed until the numerical results of the composite matches the reference value listed in Table 2. Once calibrated, the microconstituent material parameter is used in the following steps. The steps are as follows:

- Step 1: E1 – Fiber Longitudinal Modulus (E1f)
- Step 2: E2 – Fiber Transverse Modulus (E2f/E3f)
- Step 3: G12 – Fiber Shear Modulus (G12f/G13f)
- Step 4: F1 – Fiber Maximum Principle Stress (F1f)
- Step 5: F12 & F12(0.2%) – Matrix Weibull Continuum Damage (M:λ and M:ν_s)
- Step 6: F2 – Average lnterphase Failure Stress (I:σ)

At the end of the procedure, the material properties for the resin, fiber, and interphase are obtained. They are shown in section 3.2. These material properties were input into the RVE finite element model in MultiMech, shown in Figure 4, and coupled with the global scale model of the coupon. The multiscale simulation was executed, considering three different layups from NIAR, as shown in Table 3. Layup 1 is a standard “quasi-isotropic” layup. Layup 2 has 50% of the plies aligned in the direction of the load, sometimes referred to as the “hard” layup. Layup 3 has primarily 45 degree plies, sometimes referred to as the “soft” layup.

Each ply was modelled as a single layer of elements, as exemplified in Figure 5. Depending on the number of plies, the model contained either 6144 or 7640 solid, 8 node linear elements. With all coupons sized according to ASTM 3039, tensile strengths were compared between each of the layups. The comparison is discussed in the next section.

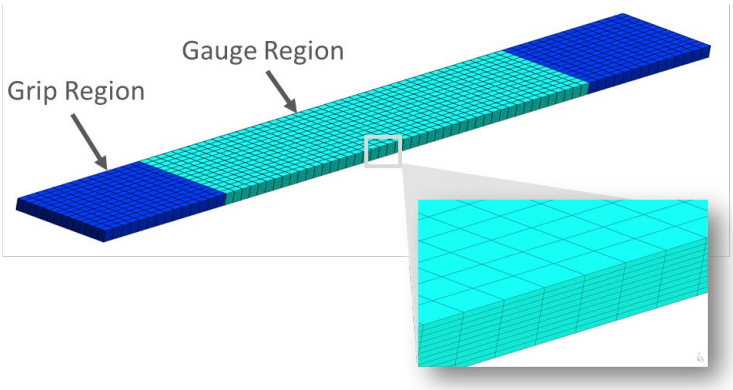


Figure 5. Mesh of the coupon used in study #2.

3. RESULTS

3.1 Study #1

Before running the coupon-scale models, the RVE finite-element models were run using MultiMech 18.1, to verify if the predicted strengths matched the reference values given [20] for each of the volume fraction bundles defined. This verification was important in ensuring the methodology of applying Weibull failure to the elements of a FE fiber will return similar results as the general fiber break model. These results, shown in Figure 6, are in good agreement between predicted and calculated values, demonstrating that the Weibull approach in the microstructure FE model is suitable.

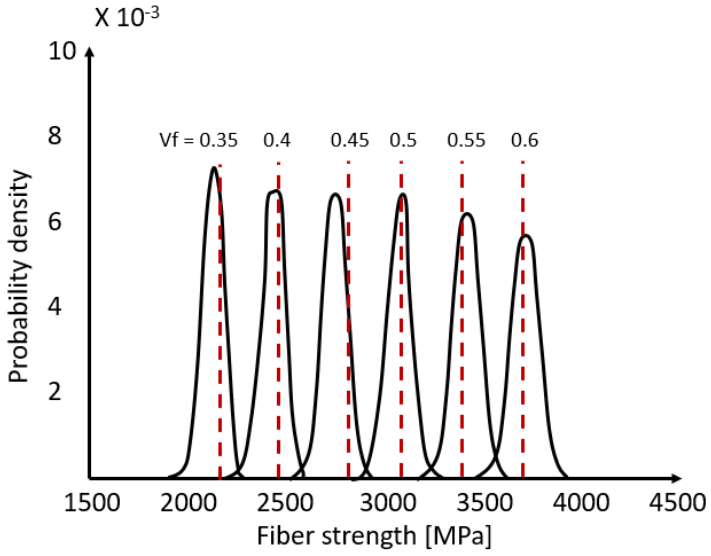


Figure 6. Comparison between fiber break model (black lines) and MultiMech RVE model (red dashes, average of 3 runs) results calculated for the strength as a function of volume fraction.

After this validation, the RVEs were input into the coupon model and a series of three simulations were run. Although the input data was the same for the three cases, the stochasticity

considered in the fiber strength led to three different results of the coupon strength, as shown in the Figure 7. These results compare very well with the reference paper, as shown in Figure 8.

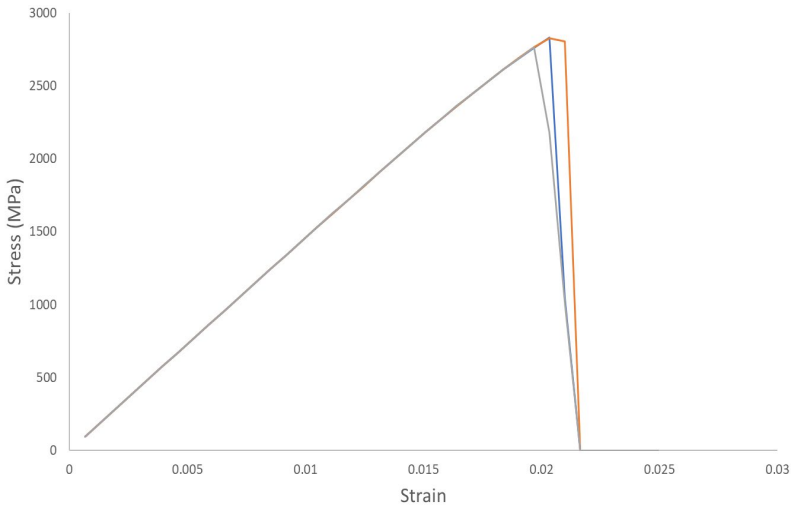


Figure 7. Stress-strain curves of the three sequential tensile tests simulated in study #1.

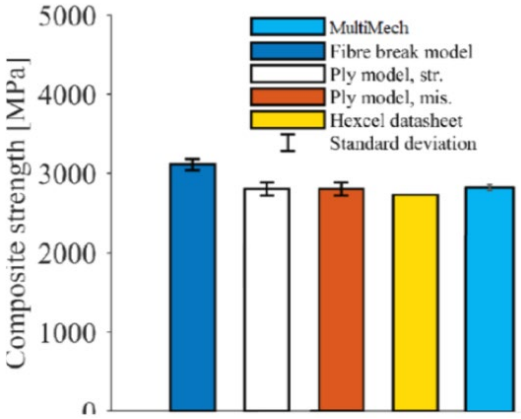


Figure 8. Comparison datasheet between MultiMech and other results.

Figure 9 compares the stress, failure, and stiffness states at three different moments of the test. Moment 1 shows the beginning of the simulation where the coupon only experiences an elastic response. Here the stiffness and stresses evolve linearly without failure in any of the RVEs. The stiffnesses and stresses can be seen coinciding with one another. At moment 2, the first group of RVEs fail, slightly associated with the higher percentage volume fraction RVEs. With this initial failure, the once load bearing RVEs transfer the stresses to neighboring RVEs. This leads to catastrophic failure at the next moment, when the second group of RVEs fails. In Moment 3, the blue and green regions in the top image indicate those areas are no longer bearing any stress.

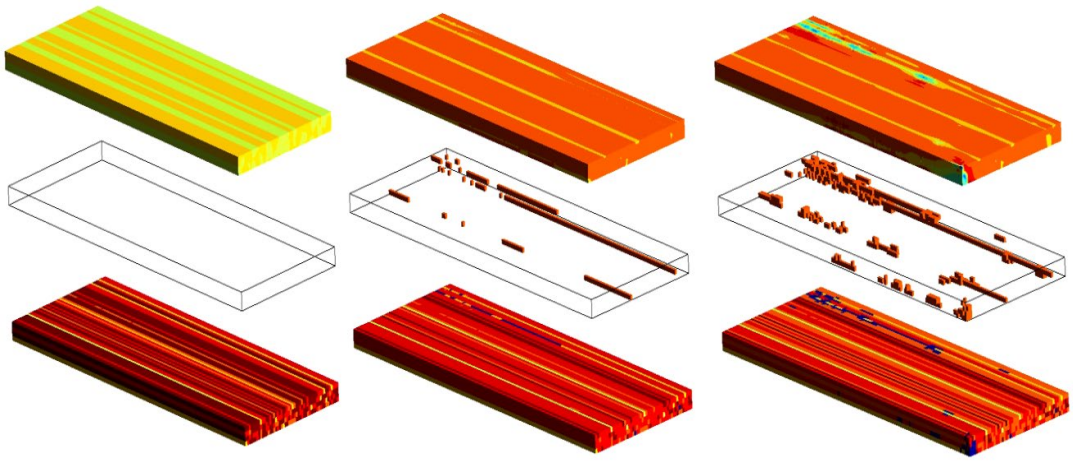


Figure 9. Longitudinal stresses (top images), element failure (middle images), and element stiffness (bottom image) at three different moments of the test. The numbers at the bottom indicate the chronological moments in the simulation.

3.2 Study #2

Like the first study, the second began by working in the RVE scale. The lamina data was used in the steps described in section 2.2 to determine the material properties of the microconstituents. The results obtained at each step are summarized in Table 2.

Table 2. Microconstituent results from the six-step calibration process.

Microconstituent Material Parameter	8552/IM7 reference parameters
E1f – Fiber Longitudinal Modulus	269.5 GPa
E2f/E3f – Fiber Transverse Modulus	16.2 GPa
G12f/G13f – Fiber Shear Modulus	12.4 GPa
F1f – Fiber Maximum Principle Stress	4195 MPa
M:λ and M:ν_s – Matrix Weibull CD	1.26 – 0.062
I:σ – Avgerage Interphase Failure Stress	30.9 MPa

The stress-strain curves for the calibrated RVE's uniaxial virtual tests are summarized in Figure 10. All virtual tests were strain controlled. These include the longitudinal test (fiber direction or 0 degree), transverse test (orthogonal to fiber direction or 90 degree), and in-plane shear test (same plane as fiber direction). For every test the different lamina target values are shown in red on the graphs. The error between the RVE results and the target lamina parameters are shown in Table 5.

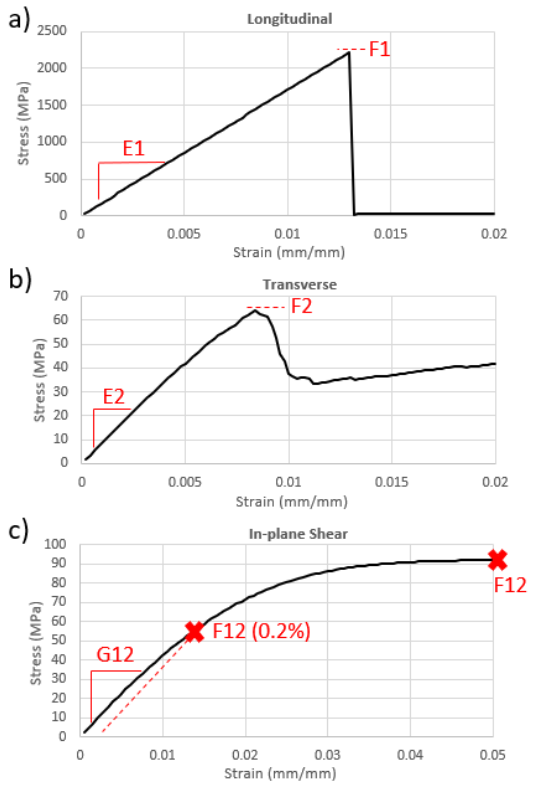


Figure 10: Stress-strain curves of the RVE virtual tests: (a) Longitudinal, (b) Transverse, and (c) In-plane Shear.

Table 3. Lamina parameters and RVE error for 8552/IM7.

Target lamina parameters	8552/IM7 NIAR lamina data	RVE Error
E1 – Longitudinal modulus	162 GPa	0.25%
F1 – Longitudinal strength	2234 MPa	0.47%
E2 – Transverse modulus	8.96 GPa	0.26%
F2 – Transverse strength	64 MPa	0.09%
G12 – In-plane shear modulus	4.69 GPa	0.20%
F12 – In-plane shear strength	91.2 MPa	1.82%
F12 (0.2%) – 0.2% shear strain offset stress	53.5 MPa	1.82%
M – Matrix modulus	4.67 GPa	N/A

The RVE error for the longitudinal and transverse cases are well under 1% error. This is due to the fact that each of the microconstituent variables of interest for the tests were isolated when being calibrated. If desired, the error could be closer to 0% error if the time step was refined further. However, the errors shown here are acceptable. For the in-plane shear strengths, the error was slightly higher. This was because two microconstituent variables of interest were being calibrated for a single test, and due to the highly coupled nature of these variables, it is more difficult to get as low of an error. However, under 2% error is sufficient.

The calibrated RVEs were then used as the input material for the coupon level models. Upon displacement controlled tensile loading, the results shown in Figure 11 were obtained:

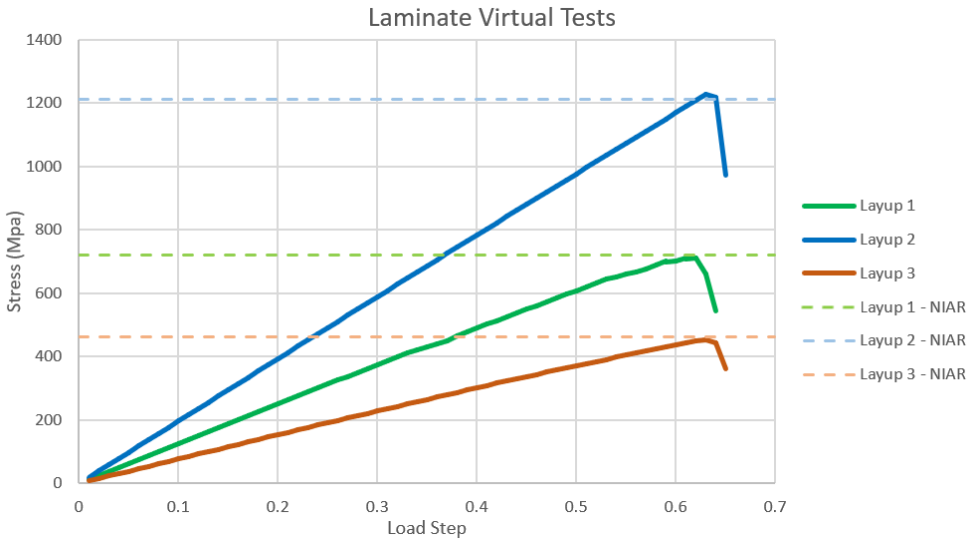


Figure 11: Stress-strain plots for the three different unnotched tension tests.

Table 4. Error between numerical models and experimental data.,

Layups for 8552-IM7	NIAR Experimental Results	Model Error
Layup 1 – [45,0,-45,90]2s	721 MPa	-1.3%
Layup 2 – [0,45,0,90,0,45,0,-45]s	1211 MPa	0.9%
Layup 3– [45,-45,0,45,-45,90,45,-45,45,-45]s	462 MPa	-1.8%

For all 3 of the layups, the error is under 2%, which is impressive given the lower accuracy of other, more common, failure models used in FE analysis of composite materials. This increase in accuracy is a result of the realistic physics being applied at the microscale. The catastrophic failure of the layups is due to the fiber failure in the 0-degree plies. Before this failure, however, the other plies demonstrate non-linear responses. For the 45-degree plies, the RVE matrix accumulates stiffness reduction, as well as slight fiber-matrix interfacial shear failure (leading to gradual stiffness reduction). For the 90-degree plies, interfacial tensile failure occurs earlier in the simulation which leads to more damage accumulated in the matrix. By representing these different failure modes, the results indicate that the individual ply's stresses are being accurately represented.

4. CONCLUSIONS

The models studied in this work support the theory that multiscale FE models can be used to improve the accuracy of FRP strength prediction. The inhomogeneity of these materials leads to complex failure mechanisms, highly anisotropic behavior, and dependence on statistical

distributions. By representing advanced composite materials through FE microstructural models in a fully coupled manner, all physics associated with these material can be accounted for and create a fully representative and accurate model.

Two different studies demonstrated the advantage of multiscaling. The first study focused on the longitudinal properties of the unidirectional FRP, where the fiber governs the composite properties through its high axial strength and stochastic strength distribution. By implementing a fiber strength distribution and FVF into the coupon model, not only was there strong model – experimental correlation, but also variation across different runs. A numerical model that demonstrates variation has the potential to replace physical experiments with virtual testing.

The second study focused more on the multiaxial behavior of the composite. The longitudinal properties of the RVE were generalized, but the other load cases (transverse and in-plane shear) were accounted for. This allowed for debonding and matrix failure to contribute to the ultimate strength of different layups. It is clear through the model – experiment results that this method accurately represents the composite plies undergoing complex loads.

Moving forward, the methods in these two studies can be combined to represent material failure in the fiber and non-fiber direction. Also, incorporating more advanced material models, like viscoelasticity, plasticity, and interlaminar failure, can help increase the accuracy of these results further and for more standardized material tests.

5. REFERENCES

1. Jones, R.M. *Mechanics of composite materials vol. 2* (Taylor & Francis London, 1975).
2. Eshelby, J.D. “The determination of the elastic field of an ellipsoidal inclusion, and related problems”. *Proceedings of the Royal Society* 241 (1957): 376-396. https://doi.org/10.1098/rspa.1957.0133
3. Mori, T., and Tanaka, K. "Average stress in matrix and average elastic energy of materials with misfitting inclusions." *Acta Metallurgica* 21(5) (1973): 571-574. https://doi.org/10.1016/0001-6160(73)90064-3
4. Hinton, M. (1998). "Predicting failure in composite laminates: the background to the exercise." *Composites Science and Technology*, 58(7), 1001–1010. https://doi.org/10.1016/s0266-3538(98)00074-8
5. Tsai, S.W., and Wu, E.M. "A general theory of strength for anisotropic materials." *Journal of Composite Materials* 5(1) (1971): 58-80. https://doi.org/10.1177/002199837100500106
6. Hashin, Z. "Failure criteria for unidirectional fiber composites." *Journal of Applied Mechanics* 47(2) (1980): 329-334. https://doi.org/10.1115/1.3153664
7. Christensen, R. M. "Stress based yield/failure criteria for fiber composites." *International Journal of Solids and Structures* 34(5) (1997): 529-543. https://doi.org/10.1016/S0020-7683(96)00038-8

8. Soden, P. (1998). "Lamina properties, lay-up configurations and loading conditions for a range of fibre-reinforced composite laminates. " *Composites Science and Technology*, 58(7), 1011–1022. https://doi.org/10.1016/s0266-3538(98)00078-5

9. Zhou, Y.-X., & Huang, Z.-M. (2012). "A bridging model prediction of the ultimate strength of composite laminates subjected to triaxial loads. " *Journal of Composite Materials,* 46(19–20), 2343–2378. https://doi.org/10.1177/0021998312449491

10. Cuntze, R. G., & Freund, A. (2004). "The predictive capability of failure mode concept-based strength criteria for multidirectional laminates." *Composites Science and Technology*, 64(3–4), 343–377. https://doi.org/10.1016/s0266-3538(03)00218-5

11. Mayes, J. S., & Hansen, A. C. (2004). "Composite laminate failure analysis using multicontinuum theory." *Composites Science and Technology*, 64(3–4), 379–394. https://doi.org/10.1016/s0266-3538(03)00219-7

12. Bogetti, T. A., Hoppel, C. P. R., Harik, V. M., Newill, J. F., & Burns, B. P. (2004). "Predicting the nonlinear response and progressive failure of composite laminates." *Composites Science and Technology*, 64(3–4), 329–342. https://doi.org/10.1016/s0266-538(03)00217-3

13. Goree, J. G., & Gross, R. S. (1980). "Stresses in a three-dimensional unidirectional composite containing broken fibers." *Engineering Fracture Mechanics*, 13(2), 395–405. https://doi.org/10.1016/0013-7944(80)90068-5

14. Hedgepeth, J. M., & Van Dyke, P. (1967). "Local Stress Concentrations in Imperfect Filamentary Composite Materials." *Journal of Composite Materials*, 1(3), 294–309. https://doi.org/10.1177/002199836700100305

15. Blassiau, S., Bunsell, A. ., & Thionnet, A. (2007). "Damage accumulation processes and life prediction in unidirectional composites." *Proceedings of the Royal Society A: Mathematical, Physical and Engineering Sciences*, 463(2080), 1135–1152. https://doi.org/10.1098/rspa.2007.1817

16. Blassiau, S., Thionnet, A., & Bunsell, A. R. (2006). "Micromechanisms of load transfer in a unidirectional carbon fibre–reinforced epoxy composite due to fibre failures. Part 1: Micromechanisms and 3D analysis of load transfer: The elastic case." *Composite Structures*, 74(3), 303–318. https://doi.org/10.1016/j.compstruct.2005.04.013

17. Kim, Y.-R., Souza, F. V., & Teixeira, J. E. S. L. (2012). "A two-way coupled multiscale model for predicting damage-associated performance of asphaltic roadways." *Computational Mechanics*, 51(2), 187–201. https://doi.org/10.1007/s00466-012-0716-8

18. Souza, F. V., & Allen, D. H. (2009). "Multiscale modeling of impact on heterogeneous viscoelastic solids containing evolving microcracks." *International Journal for Numerical Methods in Engineering*, https://doi.org/10.1002/nme.2773

19. Souza, F.V., Allen, D.H. "Modeling the transition of microcracks into macrocracks in heterogeneous viscoelastic media using a two-way coupled multiscale model". *International Journal of Solids and Structures* 48 (2011): 3160-3175. https://doi.org/10.1016/j.ijsolstr.2011.07.010

20. Malgioglio, F., Mesquita, F., Breite, C., Matveeva, A., Farkas, L., Desmet, W., Lomov, S.V., Swolfs, Y. "Prediction of tensile stiffness and failure of carbon fibre composite

laminae: a multi-scale non-deterministic approach." *European Conference on Composite Materials*. Athens, Greece, June 2018.
21. Sutcliffe, M.P.F., Lemanski, S.L., Scott, A.E. "Measurement of fibre waviness in industrial composite components." *Composites Science and Technology*, 72, p. 2016-2023, 2012. https://doi.org/10.1016/j.compscitech.2012.09.001
22. National Institute for Aviation Research, *Hexcel 8552 IM7 Unidirectional Prepreg 190 gsm & 35%RC Qualification Material Property Data Report.* April, 2011 Revision A